ELSEVIER

Journal of Computational and Applied Mathematics 111 (1999) 305–317

JOURNAL OF COMPUTATIONAL AND APPLIED MATHEMATICS

www.elsevier.nl/locate/cam

Adaptive cellular integration of linearly implicit differential equations ☆

Ricardo Riaza *,[1], Pedro J. Zufiria

Depto. Matemática Aplicada a las Tecnologías de la Información, Escuela Técnica Superior de Ingenieros de Telecomunicación, Universidad Politécnica de Madrid, Spain

Received 22 March 1998; received in revised form 23 April 1999

Abstract

The use of cell-to-cell mapping methods for the global analysis of linearly implicit ODEs is addressed in this paper. Limitations of simple and adjoining cell mapping when applied to linearly implicit equations motivate the introduction of a finite-time convergence model for cellular methods, which unifies time and spatial discretization with numerical aspects in a comprehensive framework. The resulting formal characterization of some properties of simple and adjoining cell mapping leads to a hybridization of both techniques, which is shown to be well-behaved for the analysis of linearly implicit ODEs. © 1999 Elsevier Science B.V. All rights reserved.

Keywords: Cell-to-cell mapping; Spatial discretization; Linearly implicit ODEs; Impasse points

1. Introduction

Cell mapping technique is a computational method of global analysis for nonlinear dynamical systems [9,10,26,29,32]. It is based on the discretization of the state space in *cells* and, in the continuous-time case, the numerical computation of a finite number of trajectories for constructing a *cell-to-cell mapping*, which can be considered as a discrete-time, discrete-space approximation of the original flow. Cell mapping flexibility and low computational cost, as well as its global and distributed nature, have led to a wide range of applications, specially relevant among the community

☆ An earlier version of this paper was presented under the title *Adaptive cellular integration of dynamical systems constructed for locating regular and singular invariants of a given flow* in the 2nd Meeting on Numerical Methods for Differential Equations, Coimbra, Portugal, Feb. 25–27, 1998. This work was partially supported by CICYT project TAP 94-115 and MEC project PB97-0566-C02-01.

* Corresponding author.

E-mail address: rrr@mat.upm.es (R. Riaza)

[1] Supported by a fellowship from Universidad Politécnica de Madrid.

PII: S0377-0427(99)00151-X

of intelligent control (see [12] for a neural controller design and [18] for a survey on fuzzy control). Applications have also been reported in fields such as mechanics and root finding problems, among others: a sample can be found in [6,31].

Nevertheless, many reported applications of cell mapping methods suffer the lack of a formal framework oriented to a rigorous characterization of the link between the dynamics of the original system and its cellular approximation. This characterization can be properly framed around the *shadowing lemma* [1,2] and spatial discretization of dynamical systems [3–5,8,11,14–16]. See specially [3–5] and references therein for the analysis of different qualitative and statistical effects of spatial discretizations on mappings, and [14–16] for the lifting of algebraic invariants of finite representable multivalued maps (constructed from computer simulations or experimental data) to the original dynamical system.

In this paper, the interest is focused on the use of cell mapping methods for the global analysis of linearly implicit ordinary differential equations [13,20,21,23,25]. These equations are defined by a differential system

$$A(u)\dot{u} = f(u), \tag{1}$$

where $A \in C^k(\mathbb{R}^n, \mathbb{R}^{n\times n})$, being $\mathbb{R}^{n\times n}$ the set of all $n\times n$ real matrices, and $f \in C^l(\mathbb{R}^n, \mathbb{R}^n)$, with $k, l \geqslant 1$. This is motivated by the interest in analyzing the stability properties of different discretizations of the continuous Newton method [7,19,30,31]

$$-J(u)\dot{u} = f(u), \tag{2}$$

being J the Jacobian of f, particularly in the neighborhood of singular points, where J (or A in the general case) is non-invertible.

Systems (1) and (2) typically possess a hypersurface of *standard singularities* [20] or *impasse points* [21], where trajectories cease to exist. The attempt to integrate a trajectory beyond one of these points will necessarily give a spurious solution, which is the reason for simple cell mapping (scm) [9,10] not being adequate for the analysis of these systems [30]. Nevertheless, these singularities have a special significance in the global dynamics of the system, and therefore its global analysis via cellular methods requires a modification of these tools to handle impasse points. Adjoining cell mapping (acm) [30,32] displays a better behavior regarding this topic, but some peculiar effects produced by this cellular method point out the necessity of formal results providing a framework for the analysis of cellular tools. In this direction, the present paper introduces a finite-time convergence model for cell-to-cell mappings, which takes account of the following aspects:

1. *Time discretization*: the choice of an integration time T for converting a flow into a discrete map is the starting point of cellular methods for continuous-time dynamical systems. This issue is not present when the problem is directly addressed in the discrete-time setting [3–5]. Impasse points of linearly implicit ODEs motivate the choice of this integration time in a state-dependent or *adaptive* manner, as it is done in acm.
2. *Spatial discretization*: the cellular error introduced by cell algorithms is covered by the *shadowing lemma* [1,2], and will be shown to be linearly dependent on the cell size l.
3. *Numerical integration* provides another source of error: the relative incidence of the numerical step h and the cell size l in the global error must be studied. Special care must be taken when integrating trajectories near impasse points [21,24].

The convergence model to be introduced will lead to a hybridization of scm and acm into a new cellular tool, oriented to linearly implicit ODEs (namely, *hybrid cell mapping* or hcm). Hcm retains the convergence of scm but behaves adaptively, as acm, near standard singularities. As the cellular size approaches zero, hcm behaves as scm, truncating trajectories which reach impasse points.

The paper is structured as follows. The fundamentals of scm and acm are compiled in Section 1.1. Section 1.2 summarizes some properties of linearly implicit ODEs. Section 2 presents a finite-time convergence model for cell mapping methods: scm and acm are analyzed in the light of this theory. As mentioned above, the use of an underlying numerical method for the integration of trajectories is also considered, leading to a unified treatment of both cellular and numerical aspects. Hcm is introduced in Section 3 as a new cellular technique obtained through the hybridization of scm and acm. Finally, concluding remarks are summarized in Section 4.

1.1. Simple and adjoining cell mapping

The goal of cell mapping methods is to approximate the dynamics of a given system

$$\dot{u} = F(u),\ u \in \Omega \subset \mathbb{R}^n, \quad F \in C^p(\Omega, \mathbb{R}^n), \tag{3}$$

being the assumed regularity $p \geqslant 1$ given by the order of the numerical method to be used, by means of a *cellular dynamical system* $z_{k+1} = C(z_k)$ defined in a lattice or *cell state space* S. This state space is obtained as $S = \varphi(\Omega)$, where $\varphi : \mathbb{R}^n \to \mathbb{Z}^n$ (sometimes referred as *discretization operator* [3] or *roundoff operator* [5]) groups together all the points $u = (u^1, \ldots, u^n)$ of an n-dimensional rectangle into a single integer vector $z = (z^1, \ldots, z^n)$, through the relation

$$(z^i - 1/2)l^i \leqslant u^i - \tilde{u}^{\,i} < (z^i + 1/2)l^i, \quad i = 1, \ldots, n.$$

The parameters $l = (l^1, \ldots, l^n)$, $\tilde{u} = (\tilde{u}^{\,1}, \ldots, \tilde{u}^{\,n}) \in \mathbb{R}^n$ are known as the *cell size* and the *origin*, respectively. Note that S is a finite set if Ω is bounded. Usually, an n-dimensional rectangle $\mathscr{H} = [a_1, b_1) \times \cdots \times [a_n, b_n) \subset \Omega$ is taken as the region of study, grouping $\Omega - \mathscr{H}$ into a single cell known as the *sink cell*; in this case, it is $S = \varphi(\mathscr{H})$. In this paper, all the aspects related to the sink cell will not be considered, and the choice of the origin $\tilde{u}$ will be performed randomly.

Although there exist several possibilities for defining C, we will restrict the discussion to maps of the form

$$C = \varphi \circ \Phi_{T(z)} \circ \gamma, \tag{4}$$

where $\gamma : \mathbb{Z}^n \to \mathbb{R}^n$ denotes the *center point map* $\gamma(z) = \sum_{i=1}^{n} (\tilde{u}^{\,i} + l^i z^i)\mathrm{e}^i$ (being e^i the ith vector of the canonical basis in $\mathbb{R}^n$), and Φ_T is the T-time flow associated with (3). Situations in which the flow is not defined for a given T will be extensively addressed later. The expression $\Phi_{T(z)}$ indicates that the integration time will, in general, be dependent on the cell z. The way in which the choice of $T(z)$ is accomplished defines a specific cell mapping method.

In practice, numerical computation of the trajectories must be performed and, instead of $\Phi_{T(z)}$, only a numerical approximation $\hat{\Phi}_{T(z)}$ is available, leading to a *numerical cell mapping*

$$\hat{C} = \varphi \circ \hat{\Phi}_{T(z)} \circ \gamma. \tag{5}$$

All along the paper, the use of a one-step s-stage explicit method

$$\hat{u}^{\,j+1} = G(\hat{u}^{\,j}), \tag{6}$$

will be assumed for simplicity, being $\hat{u}^j$ the points of the numerical approximation of a trajectory $u(t)$ with $u(0)=\hat{u}^0$, calculated through the evaluation of F at the *stage values* $\hat{u}^{j,1},\ldots,\hat{u}^{j,s}$. When a fixed stepsize h verifying $T(z)=\eta(z)h$, $\eta(z)\in\mathbb{N}$, is used, we get $\hat{\Phi}_{T(z)}=G^{(\eta(z))}$, where $G^{(\eta)}$ stands for the η-fold composition of G.

Simple cell mapping (scm) [9,10] is obtained when a user-defined, constant integration time T_s is chosen for all the cells in S. The defining map of scm is then

$$C_s=\varphi\circ\Phi_{T_s}\circ\gamma \tag{7}$$

and, if a one-step method as (6) with fixed stepsize $h=T_s/\eta$ (for some positive integer η) is employed, we are led to *numerical simple cell mapping* (nscm):

$$\hat{C}_s=\varphi\circ G^{(\eta)}\circ\gamma. \tag{8}$$

Among the main properties of scm and nscm we may point out their global and distributed nature, as well as the low computational cost in the construction of $\hat{C}_s$ and the existence of efficient algorithms for the global analysis of the dynamics [10], particularly for computing basins of attraction of asymptotically stable invariants. In this regard, it is also remarkable their capability for detecting asymptotically stable equilibrium points (a.s.e.p.) (resp. a.s. periodic solutions) as fixed (resp. periodic) cells or small invariant attracting sets. In the specific case of equilibria, it is easily shown that, choosing the cell size l small enough and the integration time T_s sufficiently large, an a.s.e.p. leads to an invariant cellular group. If this invariant group is a single attracting fixed cell, the cellular mapping is termed *dynamically robust* [5].

Scm and nscm have nevertheless some limitations which may be summarized as follows:

1. Existence of spurious fixed and periodic cells [10]. In particular, regions of slow dynamics (meaning $\|F\|\ll\|l\|/T_s$, where $\|u\|$ stands for $\max_{i=1,\ldots,n}\{|u^i|\}$) may lead to fixed cells not corresponding to true equilibrium points. It is immediate that, since Φ_{T_s} is a diffeomorphism, there exist a sufficiently small cell size l such that a given non-equilibrium u^* necessarily leads to a non-fixed cell. This can be combined with an adaptive enlargement of the integration time to reduce the amount of spurious fixed cells, as in acm or hcm.
2. Finite time trajectories (namely, maximal solutions defined on an interval (a,b) with $b<\infty$ and/or $a>-\infty$), may lead to fake jumps in $\hat{C}_s$. This is the case of impasse points of linearly implicit ODEs [20,21], which will be addressed later.
3. The borders of the attraction domains of a.s.e.p. are generally not well delineated in the simple cellular approximation. This effect may be reduced by using the (more costly) techniques of *generalized cell mapping* [10] or *interpolated cell mapping* [29].

In addition, the spatial error introduced by the cellular approximation must be taken into account: this topic will be considered in Section 2, within the finite-time convergence model for cell mapping methods.

Adjoining cell mapping (acm) [30,32] avoids the arbitrary selection of the integration time $T(z)$ by choosing it adaptively for each cell in S. The criterion for this choice makes use of the concept of *cell distance* $d(z,z')=\max_{i=1,\ldots,n}\{|z^i-z'^i|\}$. Two cells z, z' are said to be *adjoining* if $d(z,z')=1$, and T is an *adjoining cell time* for a cell z if $\varphi\Phi_T\gamma(z)$ is an adjoining cell of z. In acm, the map C_a is constructed trying to force the relation $d(z,C_a(z))=1$, that is, the integration time $T_a(z)$ must be an adjoining cell time for z whenever possible. The adjoining cell time finding algorithm [30]

makes use of two user parameters T_{ini} and $T_{\max}$ and performs a search of an adjoining cell time for every $z \in S$ in two stages: firstly, a linear-increase process searches for a positive integer k such that the cells $z' = \varphi\Phi_{(k-1)T_{\text{ini}}}\gamma(z)$ and $z'' = \varphi\Phi_{kT_{\text{ini}}}\gamma(z)$ verify $d(z,z') = 0$, $d(z,z'') \geqslant 1$. If the condition $kT_{\text{ini}} > T_{\max}$ is reached, then $T_a(z) = T_{\max}$ and $C_a(z) = z$; otherwise, if $d(z,z'') = 1$, set $T_a(z) = kT_{\text{ini}}$ and $C_a(z) = z''$, while $d(z,z'') > 1$ leads to a halving scheme in $[(k-1)T_{\text{ini}}, kT_{\text{ini}}]$ until an adjoining cell z_a and an adjoining cell time T_a are obtained (see [30] for details). Acm may then be described by

$$C_a = \varphi \circ \Phi_{T_a(z)} \circ \gamma. \tag{9}$$

As in scm, numerical computation of the trajectories will generally be necessary, leading to *numerical adjoining cell mapping* (nacm) $\hat{C}_a$.[2]

When compared with scm and nscm, acm and nacm provide an improvement with regard to the above-enunciated limitations: the choice of $T_{\max} \gg T_s$ reduces considerably the amount of spurious fixed cells; the adjoining requirement avoids big jumps by reducing automatically the integration time (and, internally, the stepsize h) when $\|F\|$ grows rapidly, as it happens at finite time trajectories approaching impasse points. These singularities are typically detected as pairs of adjoining 2-periodic cells. Nevertheless, acm and nacm present some drawbacks which will be analyzed in Section 2.

1.2. Linearly implicit differential equations

Linearly implicit or *quasilinear* ordinary differential equations (1) have been qualitatively studied in several recent works (see [13,20,23,25] and references therein). Computational studies can be found in [21,24]. The aforementioned references report applications in fields such as nonlinear electrical circuits, phase transitions and plasticity, among others. These equations can also model the dynamics of different methods for root-finding and optimization problems formulated from time-discretizations or modifications of the continuous Newton method, which admits a linearly implicit formulation as the one indicated in (2). Finally, differentiation procedures together with the introduction of additional variables allows for the analysis of general implicit ordinary differential equations (including nonautonomous problems) within this framework [20].

Regular points of system (1), in which $A(u)$ is invertible, define an open set $\Omega \in \mathbb{R}^n$ where the dynamic behavior of (1) is characterized by the vector field $F(u) = A^{-1}(u)f(u)$, falling in the framework indicated by (3), while the set of singular points $\Psi = \mathbb{R}^n - \Omega$ requires a more elaborated study. Rabier [20] analyzes the dynamic behavior of system (1) near *standard singular points*, namely, singularities u^* where $\nabla \det A(u^*)g(u^*) \neq 0$, being $g(u) = \operatorname{Adj} A(u)f(u)$ and denoting as $\operatorname{Adj} A$ the adjoint matrix (transpose of the matrix of cofactors) of A. He shows that (1) has exactly two solutions with $u(0) = u^*$ in $C^0([0,t_0],\mathbb{R}^n) \cap C^1((0,t_0],\mathbb{R}^n)$, both defined either for some $t_0 > 0$ or $t_0 < 0$ (being in this case $[0,t_0]$ understood as $[t_0,0]$). The singularity u^* behaves as an *impasse point* [21], where solutions are no longer defined, being either a "repelling" ("inaccessible" in [21]) or an "attracting" ("accessible") point if $t_0 > 0$ or $t_0 < 0$, respectively. Standard singularities are the most common type of singular points and typically define a hypersurface in the state space.

The attempt to numerically integrate a trajectory beyond an accessible impasse point leads necessarily to a spurious solution, and therefore this integration must be continuously monitored to

[2] In the numerical case, the stepsize h is kept constant during the linear-increase process and halved in each iteration of the halving scheme.

detect this type of singularities. This is the approach followed in [21,24], where a scalar quantity is evaluated along the trajectory for this purpose. When the numerical method is embedded in a cell-to-cell mapping, the integration time T for the involved cells must be adaptively chosen, avoiding integration beyond impasse points. Details will be given in Section 3.

Further works [23] extend the results of Rabier to situations where $g(u^*) \neq 0$ but not necessarily $\nabla \det A(u^*)g(u^*) \neq 0$, giving normal forms for system (1), while others [13,25] address the case $g(u^*) = 0$ under the assumption of hyperbolicity of $g'(u^*)$.

In the present paper, we aim to computationally analyze via cell mapping methods the existence of asymptotically stable equilibria of linearly implicit systems, as well as estimate their basins of attraction, extending the works [7,30,31]. Particular attention is paid to the case of singular equilibria, where $f(u^*) = 0$ with $u^* \in \Psi$. This singular root-finding problem presents specific difficulties, as it happens in usual discrete, homotopic and optimization methods [17] employed for tackling it. Impasse points will be shown to have a drastic incidence in the basins of attraction of asymptotically stable equilibria, and therefore their correct computational treatment is mandatory for characterizing the global behavior of these systems.

An specific case of study will be analyzed employing the different cellular methods discussed in this paper. It is defined by the continuous Newton method associated with

$$f(x, y) = (x^2 - x^4, x^5 + y^2 - 1),$$

which has five zeros located at $(-1, \pm\sqrt{2})$, $(0, \pm 1)$ and $(1, 0)$. The singular set Ψ is defined by the equation $4xy(1 - 2x^2) = 0$ and the Newton field associated with f is

$$F(x, y) = \left(\frac{x(x^2 - 1)}{2(1 - 2x^2)}, \frac{-x^7 + 3x^5 + 4x^2y^2 - 4x^2 - 2y^2 + 2}{4y(1 - 2x^2)} \right),$$

being smoothly defined in $\mathbb{R}^2$ except at the straight lines $x = \pm\sqrt{2}/2$ and $y = 0$. The regular roots $(-1, \pm\sqrt{2})$ lead to (a.s.) equilibrium points of the Newton field, as it also happens with the two singular roots $(0, \pm 1)$. Finally, the root $(1, 0)$ leads to an a.s. *directional* equilibrium point, locally possessing a cone-shape region of attraction; this phenomenon has already been characterized in the context of the discrete Newton method [22].

The comparative analysis of the different cellular tools to be considered in this paper will be illustrated through the study of the domains of attraction associated with the equilibrium points in this example. Fig. 1 delineates an approximation of these domains, obtained with nscm ($T_s = 1.0$, $l^1 = l^2 = 0.01$) and nacm ($T_{\text{ini}} = 0.2$, $T_{\max} = 4.0$, $l^1 = l^2 = 0.01$). Classical fourth-order Runge–Kutta method is employed in the simulations, for the sake of simplicity in the implementation of the singularity detection algorithm to be presented in Section 3. Both cellular methods detect the equilibrium points of the system as fixed cells; nevertheless, nscm does not succeed in approximating the cone-shape attraction domain of the root located at $(1, 0)$. This is due to the existence of a manifold of accessible impasse points in the neighborhood of this point, and the numerical integration beyond these singularities produces spurious jumps, avoiding a clear picture of the borders of the different attraction domains. Nacm, on the contrary, does not present these limitations, being the blank zone near $x = -\sqrt{2}/2$, $y = 0$ due to the existence of finite-time trajectories (not converging to $(0, \pm 1)$) in this region. The cone-shape attraction domain is approximated by nacm, but a tendency to display the borders of this domain as straight lines is suggested. This phenomenon will be analyzed further in Section 2.

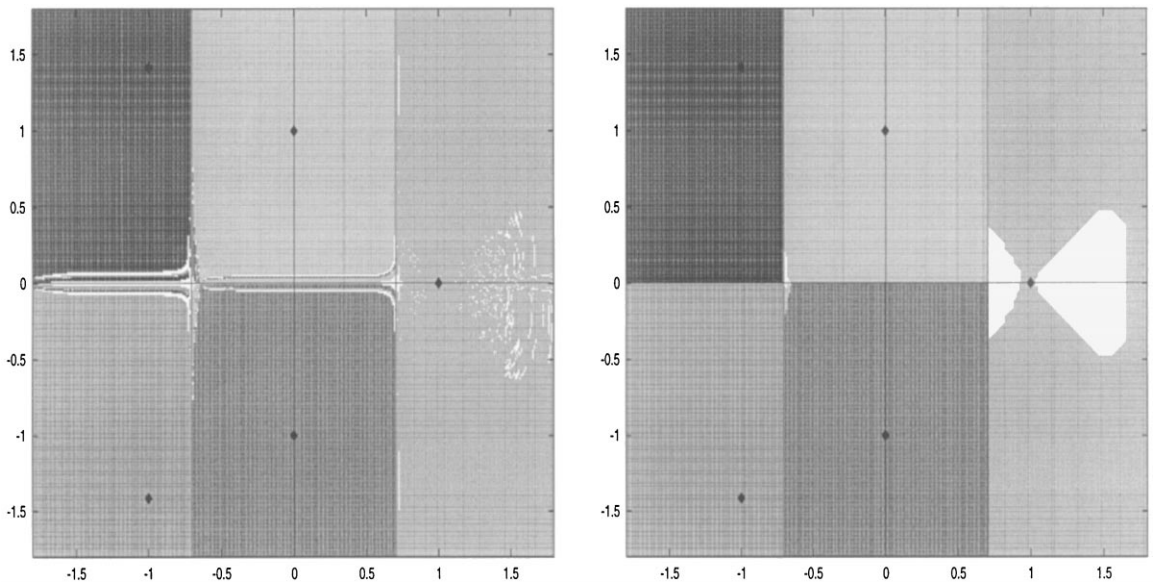

Fig. 1. Domains of attraction: (a) nscm, (b) nacm.

2. A finite-time convergence model for cell mapping methods

In this section, a convergence model for cell mapping methods is presented. The aim of this model is to characterize the approximation properties over finite time intervals of different cellular tools as the cell size $l \to 0$, taking account of the use of a numerical method for the computation of trajectories. Scm and acm, as well as their numerical counterparts nscm and nacm, will be analyzed in the light of this theory.

Let $u(t)$ denote a trajectory $u : [0,\tau] \to \Omega$ of system (3) through $u(0) = u_0$, with $\tau > 0$ fixed. A *cellular approximation* of $u(t)$, obtained by a cell mapping method (4) (or by a numerical cell mapping method (5)) with cell size l (and stepsize h in the numerical case), is a sequence $\sigma(l) = \{z_0(l), z_1(l), \ldots, z_{\kappa(l)}(l)\}$ (resp. $\sigma(l,h) = \{z_0(l,h), z_1(l,h), \ldots, z_{\kappa(l,h)}(l,h)\}$) such that:

1. $z_0 = \varphi(u_0)$, $z_k = C(z_{k-1})$ (resp. $z_k = \hat{C}(z_{k-1})$), $k = 1, \ldots, \kappa$.

2. $\sum_{k=0}^{\kappa-2} T(z_k) < \tau \leqslant \sum_{k=0}^{\kappa-1} T(z_k)$.

With the notation $T_0 = 0$, $T_k = \sum_{i=0}^{k-1} T(z_i)$, $k = 1, \ldots, \kappa$, condition 2 may be simply expressed as $T_{\kappa-1} < \tau \leqslant T_\kappa$. In scm, it is $T(z_k) = T_s$ for every cell, independently of l, and so κ will also be independent of l. Therefore, it is $T_k = kT_s$, $k = 0, \ldots, \kappa$. In acm, on the contrary, $T(z_k)$ as well as κ will be dependent on l; it may be easily proved that, in acm, $T_{\kappa(l)} \to \tau$ as $l \to 0$.[3]

For abbreviation, let $u_k = u(T_k)$, $k = 0, \ldots, \kappa - 1$, $u_\kappa = u(\tau)$, and $v_k = \gamma(z_k)$, $k = 0, \ldots, \kappa$. Note that $z_0 = \varphi(u_0)$ and so $v_0 = \gamma\varphi(u_0)$, but maybe $z_k \neq \varphi(u_k)$ and therefore $v_k \neq \gamma\varphi(u_k)$ for $k > 0$, because the points u_k belong to the actual trajectory u while v_k are the center points of the cellular approximation σ (see Fig. 2(a)).

[3] If u_0 is an equilibrium point, this relation holds if $\tau = kT_{\max}$ for some integer k.

Define the *k-step error* $e_k = \| u_k - v_k \|$, and let $e(l) = \max_{k=0,\dots,\kappa}\{e_k\}$ (in the numerical case, e will also be dependent on h and so we will denote $e(l,h)$).

Definition 1. A cell mapping method is said to be τ-convergent if $e(l) \to 0$ as $l \to 0$ for any trajectory of (3) defined on an interval $[0,\tau]$.

Definition 2. A (one-step) numerical cell mapping method is said to be τ-convergent if $e(l,h) \to 0$ as $l,h \to 0$ for any trajectory of (3) defined on an interval $[0,\tau]$, and any convergent (one-step) numerical method.

The following result can be understood as a cellular analog to the *shadowing lemma* [1,2], incorporating the effect of numerical integration.

Theorem 3. *Scm and nscm are τ-convergent for $\tau = \kappa T_s$, $\kappa \in \mathbb{N}$.*

Proof. A numerical method of order $p \geqslant 1$ will be assumed, since the non-numerical case leads to a straightforward simplification of the proof. Let δ_k be small enough for the compact set $\Phi([0,T_s] \times \bar{B}(u_k,\delta_k)) = \bigcup_{t\in[0,T_s]} \Phi_t(\bar{B}(u_k,\delta_k))$ to be in Ω, $k = 0,\dots,\kappa-1$. From [28, Theorem 2.1.12] and [27, Theorem 7.2.2.3], it may be easily proved the existence of positive constants L_k, N_k such that:

$$\| u_k - u_k' \| \leqslant \delta_k \Rightarrow \| \Phi_{T_s}(u_k) - \Phi_{T_s}(u_k') \| \leqslant e^{L_k T_s} \| u_k - u_k' \|$$

and

$$\| \Phi_{T_s}(u_k') - \hat{\Phi}_{T_s}(u_k') \| \leqslant \frac{N_k(e^{L_k T_s} - 1)}{L_k} h^p.$$

Fix $\delta = \min_k\{\delta_k\}$, $L = \max_k\{L_k\}$, $N = \max_k\{N_k\}$, and choose l_0, $h_0 > 0$ such that

$$(1 + e^{LT_s} + \cdots + e^{(\kappa-1)LT_s})\frac{\| l_0 \|}{2} + \frac{N(e^{(\kappa-1)LT_s} - 1)}{L} h_0^p = \delta.$$

Then, for any l verifying $\| l \| \leqslant \| l_0 \|$ and $h \leqslant h_0$, the following relations hold:

$$e_0 = \| u_0 - v_0 \| = \| u_0 - \gamma\varphi(u_0) \| \leqslant \frac{\| l \|}{2} \leqslant \delta \leqslant \delta_0$$

$$\begin{aligned} e_1 = \| u_1 - v_1 \| &= \| \Phi_{T_s}(u_0) - \gamma\varphi(\hat{\Phi}_{T_s}(v_0)) \| \\ &\leqslant \| \Phi_{T_s}(u_0) - \Phi_{T_s}(v_0)) \| + \| \Phi_{T_s}(v_0) - \hat{\Phi}_{T_s}(v_0)) \| + \| \hat{\Phi}_{T_s}(v_0) - \gamma\varphi(\hat{\Phi}_{T_s}(v_0)) \| \\ &\leqslant e^{LT_s} \| u_0 - v_0 \| + \frac{N(e^{LT_s} - 1)}{L} h^p + \frac{\| l \|}{2} \\ &\leqslant (1 + e^{LT_s})\frac{\| l \|}{2} + \frac{N(e^{LT_s} - 1)}{L} h^p \leqslant \delta \leqslant \delta_1 \end{aligned}$$

$$\begin{aligned} e_2 = \| u_2 - v_2 \| &\leqslant e^{LT_s} \| u_1 - v_1 \| + \frac{N(e^{LT_s} - 1)}{L} h^p + \frac{\| l \|}{2} \\ &\leqslant e^{LT_s}\left[(1 + e^{LT_s})\frac{\| l \|}{2} + \frac{N(e^{LT_s} - 1)}{L} h^p\right] + \frac{N(e^{LT_s} - 1)}{L} h^p + \frac{\| l \|}{2} \end{aligned}$$

$$= (1 + e^{LT_s} + e^{2LT_s})\frac{\| l \|}{2} + \frac{N(e^{2LT_s} - 1)}{L}h^p \leqslant \delta \leqslant \delta_2$$

$$\vdots$$

$$e_{\kappa-1} = \| u_{\kappa-1} - v_{\kappa-1} \| \leqslant (1 + e^{LT_s} + \cdots + e^{(\kappa-1)LT_s})\frac{\| l \|}{2} + \frac{N(e^{(\kappa-1)LT_s} - 1)}{L}h^p \leqslant \delta \leqslant \delta_{\kappa-1}$$

$$e_{\kappa} = \| u_{\kappa} - v_{\kappa} \| \leqslant (1 + e^{LT_s} + \cdots + e^{\kappa LT_s})\frac{\| l \|}{2} + \frac{N(e^{\kappa LT_s} - 1)}{L}h^p = K_1 \| l \| + K_2 h^p.$$

Hence $e(l,h) \leqslant K_1 \| l \| + K_2 h^p \to 0$ as $l, h \to 0$. For scm, $e(l) \leqslant K_1 \| l \| \to 0$ as $l \to 0$. □

The bound obtained suggests a result of linear convergence of scm and nscm with respect to $\| l \|$. In fact, a simple example as $\dot{x} = 1,\ \dot{y} = 0$ proves that convergence of scm and nscm can not be superlinear. Using a method of order $p > 1$, the numerical error can be easily made negligible when compared with the cellular one; in practice, a prescribed tolerance $\epsilon \ll \| l \|$ in some standard numerical code can be used to guarantee this since, statistically, the cellular error should not be expected to be less than $\| l \| /4$.

If κ is such that $(\kappa-1)T_s < \tau < \kappa T_s$, the error e tends to $\| u(\tau) - u(\kappa T_s) \|$ which will be generally greater than zero. This is the reason for scm and nscm not being convergent when τ is not an integer multiple of T_s. Acm and nacm do not have this limitation since, as already mentioned, $T_{\kappa(l)} \to \tau$ as $l \to 0$, but this property is based on the fact that $\kappa(l) \to \infty$ as $l \to 0$, what makes acm (and nacm) non-convergent: in the counter-example $\dot{x} = 3,\ \dot{y} = 1$, the trajectory $x(t) = 3t,\ y(t) = t,\ t \in [0, \tau]$ is approximated by the sequence $z_k = (k, 0)$, being e approximately equal to τ, independently of l. This result is due to the fact that K_1 in the proof of Theorem 1 would, in the case of acm, be a sum $\frac{1}{2}\sum_{k=0}^{\kappa(l)} e^{LT_k}$, which becomes unbounded as the size of the partition $\{0, T_1, \ldots, T_\kappa\}$ tends to zero, and its product with $\| l \|$ may not tend to zero. Acm may be done convergent by introducing a third parameter $T_{\min}$ and forcing the relation $T_{\min} \leqslant T_a(z) \leqslant T_{\max}$, which, however, goes against the adjoining philosophy of the method.

Generally speaking, if square cells ($l^1 = l^2$) are used in planar systems, acm and nacm will not succeed in approximating straight lines with slope m different from $0, \pm 1, \infty$. Straight lines with $0 < |m| < 0.5$ will lead to a cellular approximation with center points in another straight line with $m = 0$, while the conditions $-2 < m < -0.5,\ 0.5 < m < 2$ and $2 < |m| < \infty$ lead to approximations with $m = -1,\ m = 1$ and $m = \infty$, respectively. Zones where the trajectories are close to straight lines will be affected by an error essentially independent of the cell size: this is the reason for the *straight line effect* observed in Fig. 1(b). A high resolution application of nacm does not improve the results (Fig. 2(b), $T_{\text{ini}} = 0.1,\ T_{\max} = 4.0,\ l^1 = l^2 = 0.00175$). An analogous effect will happen in higher dimension. Nevertheless, adjoining methods have proved their efficiency in unraveling pathological dynamics by automatically reducing the integration time (and, internally, the stepsize) in zones with fast changes in the vector field, as it is the case near impasse points of linearly implicit ODEs; this was illustrated through the improvement provided by nacm with respect to nscm (Fig. 1). These considerations have led to a hybridization of scm and acm, which preserves the convergence of scm as well as the good properties of acm when dealing with singular dynamics. This new cellular tool is presented in the next section.

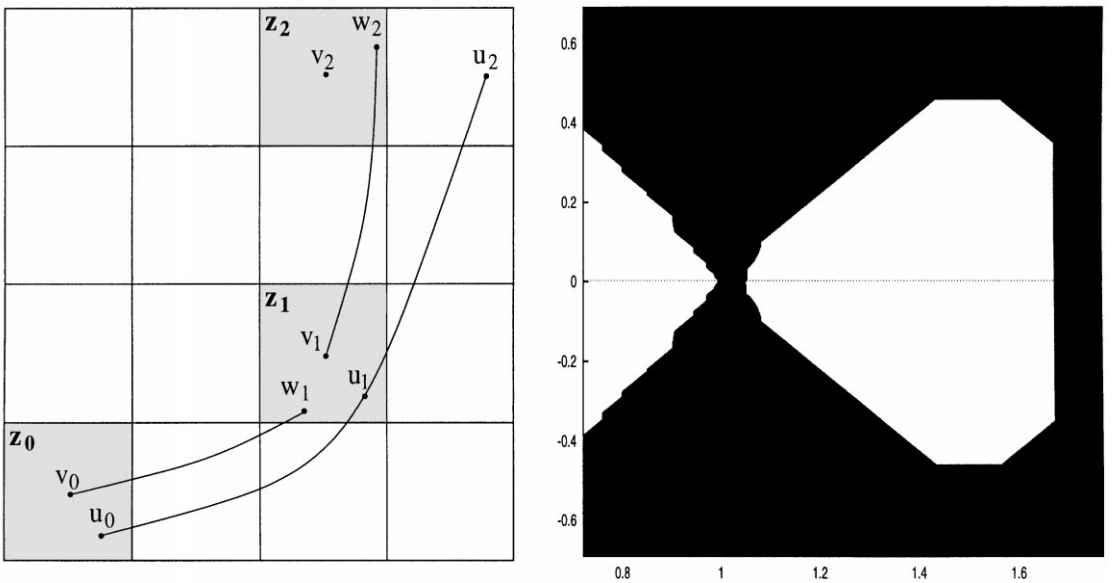

Fig. 2. (a) Cell sequence, $z_0 = \varphi u_0$, $v_i = \gamma z_i$, $w_{i+1} = \Phi_{T(z_i)} v_i$, $u_{i+1} = \Phi_{T(z_i)} u_i$, $z_{i+1} = \varphi w_{i+1}$. In the numerical case, it is $\hat{w}_{i+1} = \hat{\Phi}_{T(z_i)} v_i$, $z_{i+1} = \varphi \hat{w}_{i+1}$. (b) High resolution detail with nacm.

3. Hybrid cell mapping

In Section 2, a basic result of convergence has been proved for scm. Nevertheless, this cellular method has several drawbacks when dealing with linearly implicit systems (1), as indicated in previous sections. The adjoining requirement of acm reduces considerably these limitations, displaying however the disadvantage of non-convergence, as shown in Section 2. It is therefore natural to apply acm only in a neighborhood of the singular set Ψ. This idea leads to *hybrid cell mapping* (hcm), which is a new cellular method oriented to linearly implicit ODEs.

Hcm is obtained as a combination of scm and acm, and essentially particularizes to scm when applied to dynamical systems without singularities. Although hybrid cell mapping may be described without reference to an underlying numerical method, we will restrict our attention to *numerical hybrid cell mapping* (nhcm), which makes use of a one-step s-stage explicit numerical method as the one indicated in (6). Nhcm falls in the framework described in (5), and therefore may be characterized through a map

$$\hat{C}_h = \varphi \circ \hat{\Phi}_{T_h(z)} \circ \gamma. \tag{10}$$

When dealing with linearly implicit systems, the existence of accessible or inaccessible impasse points must be considered. Accessible impasse points u^* are reached by trajectories $u(t)$ maximally defined (in a C^1 sense) on $(t_0, 0)$, with $-\infty \leqslant t_0 < 0$, $\lim_{t \to 0^-} u(t) = u^* \in \Psi$ and $\lim_{u \to u^*} \| F(u) \| = \infty$. The attempt to numerically integrate these trajectories beyond $t = 0$ leads to big numerical jumps and a fake cellular map. Similarly, negative finite-time trajectories (maximally defined on $(0, t_0)$) leaving an inaccessible impasse point may produce big jumps when integrating forward in time from points close to the singular manifold. To detect impasse points, note that the condition $\nabla \det A(u^*) \neq 0$ at standard singularities [20] implies that Ψ is (at least locally) a hypersurface with

different signs of $\det A$ at both sides. Therefore, the algorithm will supervise the sign of $\det A$ along the computed trajectories, halting the integration as soon as a singularity is detected because of a change in this sign. This is analogous to the computational treatment of singularities in [21,24].

In outline, nhcm performs nscm steps with an internal singularity control algorithm, as mentioned above. A singularity detection forces the integration to be halted and, if the algorithm did not reach a different cell, nacm is applied. If no singularity is detected, nhcm performs T_h-integration steps (being T_h a user-defined constant) until it gets to a different cell or a prefixed maximum time $T_{\max}$ is reached. This may be formally described as follows:

1. Assume that no singularity is detected in the following integration. Set initially $T(z) = T_h$ and perform a nscm step. If $z \neq \varphi\hat{\Phi}_{T_h}\gamma(z)$, then $T_h(z) = T_h$ and $\hat{C}_h(z) = \varphi\hat{\Phi}_{T_h}\gamma(z)$. Otherwise, set $T(z) = 2T_h$ and repeat the process until $z \neq \varphi\hat{\Phi}_{kT_h}\gamma(z)$ (and then $T_h(z) = kT_h$, $\hat{C}_h(z) = \varphi\hat{\Phi}_{kT_h}\gamma(z)$) or $T_{\max}$ is reached. In this case, $T_h(z) = T_{\max}$ and $\hat{C}_h(z) = z$.
2. Suppose that a singularity is detected when performing the integration of step 1, at a given $\hat{v}^j$.[4] If $z' = \varphi(\hat{v}^{j-1}) \neq z$, set $T_h(z) = (j-1)h$ and $\hat{C}_h(z) = z'$. Else, if $z' = z$, apply nacm at z with parameters $T_{\text{ini}} = T_h$ and $T_{\max}$. It will then be $T_h(z) = T_a(z)$, $\hat{C}_h(z) = \hat{C}_a(z)$. Similarly, if a singularity is detected in a stage value $\hat{v}^{j,i}$, and $z' = \varphi(\hat{v}^j) \neq z$, set $T_h(z) = jh$ and $\hat{C}_h(z) = z'$. Else, if $z' = z$, apply nacm, being $T_h(z) = T_a(z)$, $\hat{C}_h(z) = \hat{C}_a(z)$.

The singularity detection algorithm operates by comparing the sign of $\det A(\hat{v}^0)$ with that of $\det A$ at the following evaluation points:

(a) (Forward evaluation) $\hat{v}^j$, $\hat{v}^{j,i}$, $j \geqslant 0$, $i = 1,\ldots,s$;

(b) (Backward Euler evaluation) $\hat{v}^j - hF(\hat{v}^j)$, $\hat{v}^{j,i} - hF(\hat{v}^{j,i})$, $j \geqslant 0$, $i = 1,\ldots,s$;

(c) (Transversal Euler evaluation) $\hat{v}^j \pm h\lambda_k F(\hat{v}^j)$, $j \geqslant 0$, $k = 1,\ldots,n-1$, where $\{\lambda_k\}$ is a set of operators such that $\{F(\hat{v}^j), \lambda_1 F(\hat{v}^j),\ldots,\lambda_{n-1}F(\hat{v}^j)\}$ define a orthogonal basis of $\mathbb{R}^n$ whenever $F(\hat{v}^j) \neq 0$.

Backward evaluation is used to avoid big numerical jumps near inaccessible impasse points, while transversal evaluation is oriented to non-standard singularities, where it might be $\nabla \det A = 0$. Of course, more exhaustive transversal evaluation may be used, but the one described here has been proved sufficient in several cases of study.

This algorithm classifies a cell as *singular* when nacm is applied, and *regular* otherwise. Hence, there will exist a *pseudo-regular set* $\Omega(l,h)$ and a *pseudo-singular set* $\Psi(l,h)$, obtained as the preimages through φ^{-1} of the sets of regular/singular cells. It may be easily shown that $\Omega(l,h) \to \Omega$ as $l,h \to 0$ and, hence, an analogous reasoning to that of Section 2 proves that $e(l,h) \to 0$ as $l,h \to 0$, being therefore nhcm τ-convergent for every $\tau = \kappa T_h$ with $\kappa \in \mathbb{N}$.

The application of nhcm to the case of study presented in 1.2 is shown in Fig. 3. The low resolution case (Fig. 3(a), $T_h = 1.0$, $T_{\max} = 4.0$, $l^1 = l^2 = 0.01$) displays a much better behavior than that of nscm (Fig. 1(a)), as expected, and the straight borders of the cone-shape region obtained with nacm (Fig. 1(b)) are substituted by slightly irregular lines. However, the use of a smaller cell size considerably improves the results, illustrating the convergence of nhcm. This is shown in Fig. 3(b) ($T_h = 1.0$, $T_{\max} = 4.0$, $l^1 = l^2 = 0.00175$). In fact, not only the irregularities of the borders are

[4] $\hat{v}^j = G^{(j)}(\hat{v}^0)$, $j = 0,1,\ldots$ are the points obtained in the numerical integration through $\hat{v}^0 = \gamma z$ with fixed stepsize h, while the stage values associated with $\hat{v}^j$ are denoted as $\hat{v}^{j,i}$, $i = 1,\ldots,s$.

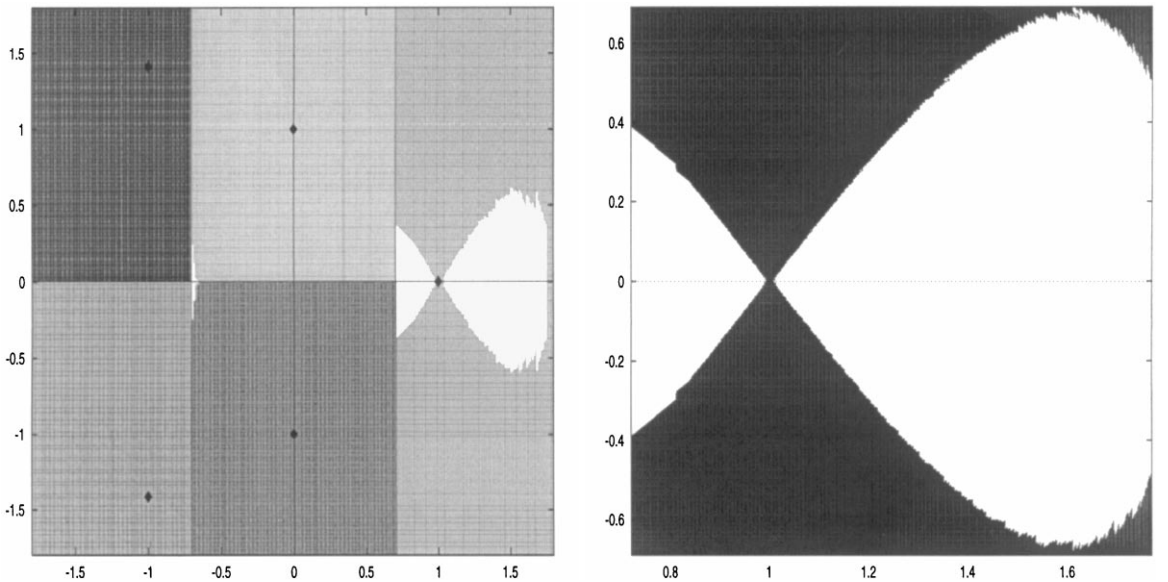

Fig. 3. Domains of attraction obtained with nhcm: (a) low-resolution (b) high-resolution detail.

significantly reduced, but also the approximation to the original dynamics is much better than the one obtained with nacm (Fig. 2(b)) using the same cell size.

4. Concluding remarks

The use of cell mapping methods for the global analysis of linearly implicit ordinary differential equations has been illustrated in this paper. These equations typically possess impasse points where standard cellular techniques (simple cell mapping) can not be applied, motivating the use of adaptive tools such as adjoining cell mapping.

Some difficulties encountered with acm have been formalized within a finite-time convergence model for cellular tools. This model clarifies the relative incidence of the time-discretization, space-discretization and numerical parameters which appear in cellular methods. A result of linear convergence for scm has been proved within this framework, and a hybridization of acm and scm has been proposed for linearly implicit equations, retaining the convergence of scm and the adaptive nature of acm for the treatment of impasse points. Some numerical experiments illustrate the scope of this new cellular tool.

References

[1] R. Bowen, Markov partitions for Axiom A diffeomorphisms, Amer. J. Math. 92 (1970) 725–747.
[2] R. Bowen, On Axiom A diffeomorphisms, CBMS Regional Conferences Series in Mathematics, Vol. 35, AMS Publications, Providence, RI, 1978.
[3] P. Diamond, P.E. Kloeden, Spatial discretization of mappings, Comput. Math. Appl. 25 (1993) 85–94.

[4] P. Diamond, P.E. Kloeden, A. Klemm, A. Pokrovskii, Basin of attraction of cycles of space discretizations of dynamical systems with SRB invariant measures, J. Statist. Phys. 84 (1996) 713–733.
[5] P. Diamond, P. Kloeden, V. Kozyakin, A. Pokrovskii, Monotonic dynamical systems under spatial discretization, Proc. AMS 126 (1998) 2169–2174.
[6] R.S. Guttalu, Steady state response of nonlinear systems by cell mapping method, The International Symposium on Advanced Computers for Dynamics and Design '89, Tsuchiura, Japan, 1989, pp. 303–308.
[7] R.S. Guttalu, P.J. Zufiria, On a class of nonstandard dynamical systems: singularity issues, in: C.T. Leondes (Ed.), Advances in Controls and Dynamic Systems, Vol. 34, Academic Press, San Diego, 1990, pp. 279–324.
[8] S.M. Hammel, J.A. Yorke, C. Grebogi, Do numerical orbits of chaotic dynamical processes represent true orbits?, J. Complexity 3 (1987) 136–145.
[9] C.S. Hsu, A theory of cell-to-cell mapping dynamical systems, J. Appl. Mech. 47 (1980) 940–948.
[10] C.S. Hsu, Cell-to-Cell Mapping: A Method of Global Analysis for Nonlinear Systems, Springer, New York, 1987.
[11] O.E. Lanford III, Informal remarks on the orbit structure of discrete approximations to chaotic maps, Exp. Math. 7 (1998) 4.
[12] T. Martínez-Marín, P.J. Zufiria, Optimal control of nonlinear systems through hybrid cell-mapping/artificial-neural-networks techniques, Int. J. Adaptive Control Signal Process. 13 (1999) in press.
[13] M. Medved, Qualitative properties of generalized vector fields, Riv. Mat. Pura Appl. 15 (1994) 7–31.
[14] K. Mischaikow, M. Mrozek, Chaos in the Lorenz equations: a computer assisted proof, Bull. AMS 32 (1995) 66–72.
[15] K. Mischaikow, M. Mrozek, Chaos in the Lorenz equations: a computer assisted proof. Part II: Details, Math. Comput. 67 (1998) 1023–1046.
[16] K. Mischaikow, M. Mrozek, J. Reiss, A. Szymczak, Construction of symbolic dynamics from experimental time series, Phys. Rev. Lett. 82 (1999) 1144–1147.
[17] J.M. Ortega, W.C. Rheinboldt, Iterative Solutions of Nonlinear Equations in Several Variables, Academic Press, New York, 1970.
[18] M. Papa, H.M. Tai, S. Shenoi, Cell mapping for controller design and evaluation, IEEE Control Systems Mag. 17:2 (1997) 52–65.
[19] H.O. Peitgen, M. Prüffer, K. Schmitt, Global aspects of the continuous and discrete Newton method: a case study, Acta Appl. Math. 13 (1988) 123–202.
[20] P.J. Rabier, Implicit differential equations near a singular point, J. Math. Anal. Appl. 144 (1989) 425–449.
[21] P.J. Rabier, W.C. Rheinboldt, On the computation of impasse points of quasi-linear differential-algebraic equations, Math. Comput. 62 (1994) 133–154.
[22] G.W. Reddien, On Newton's method for singular problems, SIAM J. Numer. Anal. 15 (1978) 993–996.
[23] G. Reiszig, H. Boche, Straightening out trajectories near singular points of implicit differential equations, Proceedings of the nineth International Symposium on System-Modelling-Control'98, Zakopane, Pl., 1998.
[24] H. von Sosen, Folds and bifurcations in the solutions of semi-explicit differential-algebraic equations, Ph.D. Thesis, Part I, California Institute of Technology, 1994.
[25] J. Sotomayor, Structurally stable differential systems of the form $A(x)x' = F(x)$, Differential Equations Dyn. Systems 5 (1997) 415–422.
[26] J. van der Spek, Cell mapping methods: modifications and extensions, Ph.D. Thesis, Eindhoven University of Technology, 1994.
[27] J. Stoer, R. Bulirsch, Introduction to Numerical Analysis, Springer, New York, 1993.
[28] A.M. Stuart, A.R. Humphries, Dynamical Systems and Numerical Analysis, Cambridge University Press, Cambridge, 1996.
[29] B.H. Tongue, K. Gu, Interpolated cell mapping of dynamical systems, J. Appl. Mech. 55 (1988) 461–466.
[30] P.J. Zufiria, Global behavior of a class of nonlinear dynamical systems: analytical, computational and control aspects, Ph.D. Thesis, University of Southern California, 1989.
[31] P.J. Zufiria, R.S. Guttalu, A computational method for finding all the roots of a vector function, Appl. Math. Comput. 35 (1990) 13–59.
[32] P.J. Zufiria, R.S. Guttalu, The adjoining cell mapping and its recursive unraveling, Part I: Description of adaptive and recursive algorithms, Nonlinear Dyn. 4 (1993) 204–226.